BIOCHEMISTRY
including biophysical chemistry & molecular biology

Article

pubs.acs.org/biochemistry

Biochemical and Structural Analysis of Inhibitors Targeting the ADC-7 Cephalosporinase of *Acinetobacter baumannii*

Rachel A. Powers,[†] Hollister C. Swanson,[†] Magdalena A. Taracila,[§,∥] Nicholas W. Florek,[†] Chiara Romagnoli,[‡] Emilia Caselli,[‡] Fabio Prati,[‡] Robert A. Bonomo,*[,§,∥] and Bradley J. Wallar*[,†]

[†]Department of Chemistry, Grand Valley State University, 1 Campus Drive, Allendale, Michigan 49401, United States

[‡]Department of Life Sciences, University of Modena and Reggio Emilia, Via Campi 183, 41125 Modena, Italy

[§]Research Service, Louis Stokes Cleveland Department of Veterans Affairs Medical Center, 10701 East Boulevard, Cleveland, Ohio 44106, United States

[∥]Departments of Medicine, Pharmacology, Molecular Biology and Microbiology, Case Western Reserve University School of Medicine Cleveland, Ohio 44106, United States

Supporting Information

ABSTRACT: β-Lactam resistance in *Acinetobacter baumannii* presents one of the greatest challenges to contemporary antimicrobial chemotherapy. Much of this resistance to cephalosporins derives from the expression of the class C β-lactamase enzymes, known as *Acinetobacter*-derived cephalosporinases (ADCs). Currently, β-lactamase inhibitors are structurally similar to β-lactam substrates and are not effective inactivators of this class C cephalosporinase. Herein, two boronic acid transition state inhibitors (BATSIs S02030 and SM23) that are chemically distinct from β-lactams were designed and tested for inhibition of ADC enzymes. BATSIs SM23 and S02030 bind with high affinity to ADC-7, a chromosomal cephalosporinase from *Acinetobacter baumannii* (K_i = 21.1 ± 1.9 nM and 44.5 ± 2.2 nM, respectively). The X-ray crystal structures of ADC-7 were determined in both the apo form (1.73 Å resolution) and in complex with S02030 (2.0 Å resolution). In the complex, S02030 makes several canonical interactions: the O1 oxygen of S02030 is bound in the oxyanion hole, and the R1 amide group makes key interactions with conserved residues Asn152 and Gln120. In addition, the carboxylate group of the inhibitor is meant to mimic the C_3/C_4 carboxylate found in β-lactams. The C_3/C_4 carboxylate recognition site in class C enzymes is comprised of Asn346 and Arg349 (AmpC numbering), and these residues are conserved in ADC-7. Interestingly, in the ADC-7/S02030 complex, the inhibitor carboxylate group is observed to interact with Arg340, a residue that distinguishes ADC-7 from the related class C enzyme AmpC. A thermodynamic analysis suggests that ΔH driven compounds may be optimized to generate new lead agents. The ADC-7/BATSI complex provides insight into recognition of non-β-lactam inhibitors by ADC enzymes and offers a starting point for the structure-based optimization of this class of novel β-lactamase inhibitors against a key resistance target.

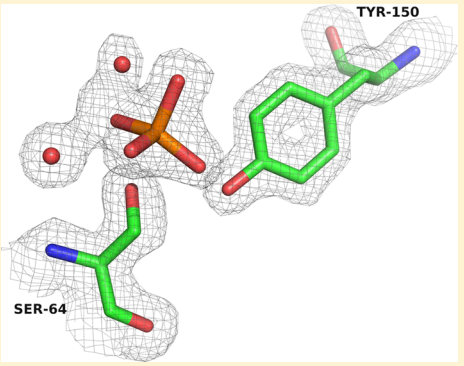

β-Lactam resistance in *Acinetobacter baumannii* presents one of the greatest and most pressing challenges to contemporary antimicrobial chemotherapy. In just the past 8 years, resistance to all classes of β-lactams (penicillins, cephalosporins, and carbapenems; Figure 1A) among clinical isolates of *A. baumannii* has significantly increased.[1−5] Varieties of mechanisms working alone and in combination (β-lactamases, porins, efflux pumps, etc.) contribute to this clinically treacherous phenotype. Among these factors, β-lactamases of multiple classes (A, B, C, and D) are the primary determinants responsible for β-lactam resistance in *Acinetobacter spp.* As a consequence, these pathogens present a serious challenge to successful antimicrobial chemotherapy, especially in patients who are elderly, immunocompromised, or most recently, suffer serious military war wounds. Mortality rates are high and disability is prolonged.[2,4,6]

A way to overcome β-lactamase-mediated resistance in *A. baumannii* is through the design of β-lactamase inhibitors (BLIs). Clavulanate, sulbactam, and tazobactam (Figure 1B) are BLIs that are commercially available and have enjoyed more than 30 years of use.[7] BLIs co-opt the mechanism of catalysis and use the chemistry that occurs between the BLI (that mimics the β-lactam) and the residues in the active site to thwart the enzyme's versatile catalytic machinery. Unfortunately, these commercially available BLIs do not inhibit the *A. baumannii* cephalosporinase effectively enough to allow the β-lactam antibiotic to reach its cellular target, the penicillin binding proteins (PBPs).[1] Although novel bridged diazabicyclo[3.2.1]-octanone non-BLIs, DBOs, are in development as potential BLIs of class C enzymes (e.g., avibactam and MK-7660), they are not yet targeted for *A. baumannii*. As a consequence, the class D

Received: July 18, 2014
Revised: November 7, 2014
Published: November 7, 2014

   dx.doi.org/10.1021/bi500887n | *Biochemistry* 2014, 53, 7670−7679

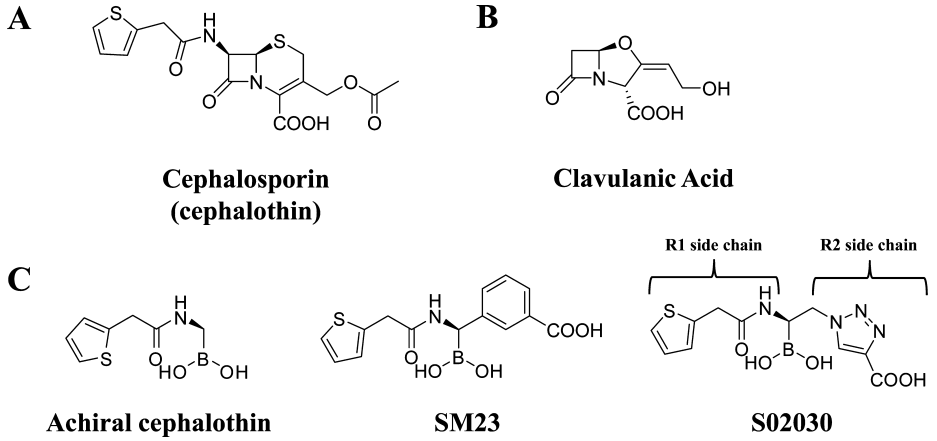

Figure 1. β-Lactamase ligands. (A) Cephalothin, a cephalosporin antibiotic. (B) Clavulanic acid, a β-lactam-based β-lactamase inhibitor (BLI). (C) Novel boronic acid transition state analog inhibitors (BATSIs).

oxacillinases, carbapenemases, and permeability factors severely limit their use.[8] New approaches in BLI design are needed to overcome this complex β-lactamase background in *Acinetobacter* spp. and this formidable clinical threat.[9]

With respect to *A. baumannii,* studies seeking to understand the mechanistic details of cephalosporinase structure−function relationships to aid in the design of novel BLIs are in their infancy. The cephalosporinase of *A. baumannii* (or *A*cinetobacter *d*erived *c*ephalosporinase, ADC) is a chromosomally encoded class C β-lactamase that is responsible for resistance to penicillins, cephalosporins, and β-lactam/BLI combinations.[10] Unlike other class C enzymes, which are inducible, ADC cephalosporinase expression is constitutive, driven by both its native promoter and insertion sequences that cause a highly expressed enzyme and minimum inhibitory concentrations (MICs) that exceed serum levels of expanded-spectrum cephalosporins. Early work on ADC-7 β-lactamase demonstrated remarkably high k_{cat} for first-generation cephalosporins and a relatively high K_m for the commercially available BLIs.[10] Importantly, substantial phylogenetic distance separated $bla_{ADC\text{-}7}$ (and other bla_{ADCs}) from *ampC* genes and supported the development of targeted therapies specific for *Acinetobacter* cephalosporinases.[9,10]

The rapid development of whole genome sequencing revealed the immense diversity of ADCs in *A. baumannii*.[11] Presently, the genetic/amino acid sequences of more than 240 unique enzymes in this class C family are catalogued. Interestingly, comparative whole genome sequencing has also shown that bla_{ADC} resides in a locus that is highly variable.[12] These observations raise the concern that sequence variability may play an important survival role in resistance to β-lactams in *A. baumannii*. The hypothesis has been advanced that the amino acids in the active site serve overlapping roles in the recognition of β-lactam antibiotics.[13] The notion of "enzyme plasticity" may explain why ADC β-lactamase variants evolve with novel or expanded catalytic properties (such as ADC-56) and remains to be tested.[14]

To provide a template for effective inhibitor design efforts against this important resistance target, we determined the X-ray crystal structure of the ADC-7 cephalosporinase. This enzyme was chosen because significant work had already been performed probing the active site with different inhibitors.[13] In studies performed previously, boronic acids were shown to be effective transition state analogue inhibitors of ADC-7 (here referred to as BATSIs).[13] Using strategically designed BATSIs, a chiral cephalothin analogue with a meta-carboxyphenyl moiety corresponding to the C_3/C_4 carboxylate of β-lactams showed the lowest K_i (21 ± 1 nM) for ADC-7 (SM23, Figure 1C). These findings led to the further development of these important BATSIs. The present analysis describes the kinetic characterization of the novel BATSI, S02030, the carboxytriazole derivative of SM23. With these important milestones, we are now poised to explore the structure/function relationship in ADC-7 for optimization of the BATSIs as important *Acinetobacter* class C inhibitors.

MATERIALS AND METHODS

Synthesis and Chemical Analysis. *General Methods.* SM23 was synthesized as already described.[15] The synthesis of the new S02030 was performed following the pathway depicted in Scheme 1. The highly stereoselective homologation of (+)-pinanediol azidomethaneboronate **2** allowed for the desired configuration at the asymmetrically substituted boron bearing carbon atom, while the azide group in **5** facilitated the formation of the triazole ring by the highly efficient copper-catalyzed azide−alkyne cycloaddition (CuCAAC). Compound **2** was obtained through chlorine substitution of **1**[16] with sodium azide, catalyzed by tetrabutylammonium iodide as the phase transfer agent (97%).[17] Subsequent treatment with *in situ* generated dichloromethyl lithium at −100 °C allowed the introduction in **3** of a halogenated carbon on the previous carbon−boron bond; the use of (+)-pinanediol as a chiral auxiliary agent allows for the desired *S* configuration with high diastereoselectivity (d.e. >98%, 96%).[18−22] Treatment with lithium bis(trimethylsilyl)amide, performed at −100 °C to minimize elimination reaction, produced the intermediate **4** (80%) with clean inversion of the configuration. This latter compound was then deprotected at nitrogen with a stoichiometric amount of methanol and coupled with thiophenacetyl chloride to afford compound **5** (62%).

For assembling the "right part of the molecule," we employed the copper-catalyzed azide alkyne cycloaddition between the azido group in **5** and propiolic acid, exploiting copper catalysis to gain regioselectivity and microwave irradiation to increase efficiency.[23−25] The synthesis of 1,4-disubstituted triazole **6** (60%) was confirmed by multinuclear bidimensional NMR spectroscopy. Final deprotection of (+)-pinanediol was accomplished by transesterification with phenylboronic acid in a biphasic system of acetonitrile/*n*-hexane,[26] to afford the

dx.doi.org/10.1021/bi500887n | *Biochemistry* 2014, 53, 7670−7679

Scheme 1. Synthesis of New BATSI Compound S02030[a]

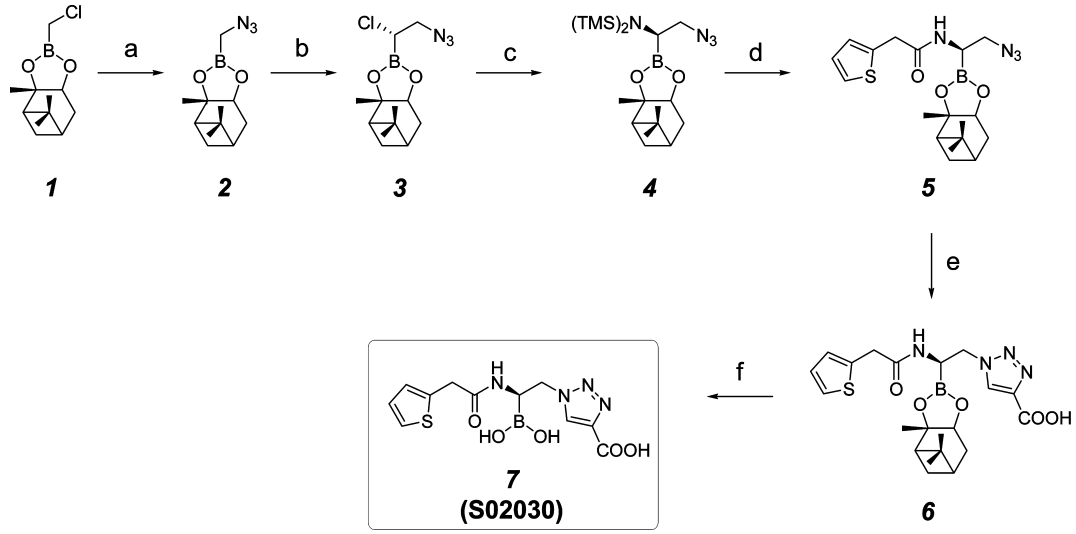

[a](a) NaN_3, TBAI, EtOAc, H_2O, r.t., overnight, 97%; (b) CH_2Cl_2, *n*-BuLi, $ZnCl_2$, THF, −100 °C → r.t., overnight, 96%, d.e .>98%; (c) $LiN(TMS)_2$, THF, −100 °C → r.t., overnight, 80%; (d) MeOH, 2-thiopheneacetyl chloride, THF, 0 °C, 1h 30 min, 62%; (e) Propiolic acid, copper in charcoal 3 wt %, 1,4-dioxane, MW, 150 °C, 30 min, 60%; (f) Phenylboronic acid, HCl, acetonitrile, *n*-hexane, r.t, 3h, 98%.

final BATSI S02030 in 98% yield.[27] NMR spectra of all intermediates are reported in the Supporting Information.

Disc Susceptibility Assays (DSAs) and Minimum Inhibitory Concentrations (MICs). DSAs were performed according to Clinical and Laboratory Standards Institute (CLSI) guidelines.[28] Bacterial cultures were grown overnight in Mueller-Hinton (MH) broth supplemented with 20 μg/mL of chloramphenicol to ensure maintenance of the β-lactamase plasmid in pBC SK (−) containing *Escherichia coli* strains. Bacterial liquid culture was then diluted using MH broth to a McFarland Standard (optical density$_{600}$ (OD_{600}) = 0.224). Bacteria were streaked onto a plate composed of MH agar and a disc containing 10 μg of compound and 10 μg of ampicillin. Plates were incubated overnight at 37 °C, and on the following day, zone sizes were measured.

Antimicrobial Susceptibility (MICs). Susceptibility profiles were determined by cation-adjusted Mueller-Hinton agar dilution MICs according to the CLSI standards previously described.[10] We employed the *E. coli* construct that was previously validated as a representative of ADC-7 in a uniform genetic background (bla_{ADC-7} was directionally cloned in pBC SK (−) phagemid vector under the control of a strong promoter) and a clinical strain *A. baumannii* M9, a multidrug resistant (MDR) strain. For the ceftazidime/BATSI combinations, the substrate concentrations were varied while the inhibitors were tested at a constant concentration of 4 μg/mL.

Protein Preparation and Purification. In order to remove the potentially disordered hydrophobic N-terminal signal peptide, a version of ADC-7 starting at amino acid 24 was subcloned into pET28a(+) (without a His-tag). The resulting plasmid that expressed amino acids D24-K383 of ADC-7 β-lactamase was transformed into the *E. coli* expression strain BL21(DE3). The cells were grown in lysogeny broth, LB, with 25 μg/mL kanamycin at 37 °C until the OD_{600} was ∼0.8. Expression of the ADC-7 β-lactamase was induced by the addition of 0.5 mM isopropyl-β-D-1-thiogalactopyranoside (IPTG). After an additional 2 h of growth at 37 °C, the cells were centrifuged (8000 rpm at 4 °C for 10 min), and the cell pellets were stored at −80 °C.

For the purification of ADC-7, cell pellets were suspended in 25 mM Tris-Cl, pH 7.0, 0.5 M NaCl with 1× HALT protease inhibitor cocktail (Sigma) and DNase I (50 Units). The solution was sonicated for 4 × 30 s intervals on ice. The lysate was centrifuged at 15000 rpm at 4 °C for 20 min. The cell-free extract (supernatant) was then mixed gently with *m*-aminophenylboronic acid resin (Sigma) for 2 h at 4 °C. The resin/supernatant mixture was poured into a column and washed with a loading buffer of 25 mM Tris-Cl, pH 7.0, 0.5 M NaCl. ADC-7 was then eluted with 0.5 M NaCl, 300 mM borate, pH 7.0. The fractions containing ADC-7 were collected, pooled, and then dialyzed in 2 × 5 L of 10 mM sodium phosphate, pH 7.0 at 4 °C. The dialyzed ADC-7 was concentrated to at least 10 mg/mL using an Amicon Ultra centrifugal filter unit with Ultra-10 membrane (Millipore). The concentration of ADC-7 was determined using the A_{280} with an extinction coefficient of 46 300 M^{-1} cm^{-1}, as calculated for the expressed residues D24-K383 of ADC-7 by the ProtParam tool on the ExPASy bioinformatics portal.[29]

ADC-7 X-ray Structure Determination. Crystals of ADC-7 were grown at room temperature via hanging drop vapor diffusion using the following conditions: ADC-7 (3 mg/mL) in 25% w/v polyethylene glycol (PEG) 1500, 0.1 M succinate/phosphate/glycine buffer at pH 5.0 (SPG buffer, Molecular Dimensions). Crystals of ADC-7 were harvested from the crystallization drop with a nylon loop and immediately cryocooled in liquid nitrogen. Data were measured from a single crystal at the LS-CAT sector (21-ID-F beamline) of the Advanced Photon Source at Argonne National Laboratory (Argonne, IL). To obtain the ADC-7/S02030 complex, preformed ADC-7 crystals were harvested and placed in a drop of well buffer supplemented with 1 mM S02030 and soaked for approximately 5−10 min before cryocooling in liquid nitrogen. The inhibitor was diluted into crystallization buffer from a 50 mM stock solution dissolved in dimethyl sulfoxide (DMSO). Data were measured from a single crystal at LS-CAT (21-ID-G beamline). Images from the apo data set

dx.doi.org/10.1021/bi500887n | *Biochemistry* 2014, 53, 7670−7679

Table 1. Thermodynamic Parameters and Affinity Constants for ADC-7/BATSI Interactions

compound	K_i[a] [nM]	K_D[b] [nM]	ΔH[b] [kcal/mol]	$-T\Delta S$[b] [kcal/mol]	ΔG[b] [kcal/mol]	T_m[b] [°C]
SM23	21.1 ± 1.9	90	−5.4 ± 0.2	−4.18	−9.61	64
S02030	44.5 ± 2.2	590	−9.3 ± 0.1	+0.82	−8.51	65

[a]Determined by kinetics experiments. [b]Determined by isothermal titration calorimetry.

were indexed, integrated, and scaled with HKL2000[30] and with XDS[31] for the complex. For the apo structure, molecular replacement was performed with Phaser[32] using a homology model generated with Phyre2.[33] This model is based on the structure of the AmpC from *Pseudomonas fluorescens* (2QZ6) and was chosen due to its high sequence identity to ADC-7.[34] For the ADC-7/S02030 complex, the apo ADC-7 structure (all waters and ions removed) was used as the initial phasing model in Phaser. Refinement was performed using Refmac5[35] in the CCP4 program suite.[36] Iterative rounds of model building were done in Coot.[37] The coordinates and structure factors for the final ADC-7 model and the ADC-7/S02030 complex are deposited with the Protein Data Bank as 4U0T and 4U0X, respectively.

Steady State Kinetics. Steady state kinetics assays were performed on a Cary 100 UV−vis spectrophotometer (Agilent Technologies) in 10 mM phosphate-buffered saline (pH 7.4) with 2 nM ADC-7. The V_{max} and K_m of the β-lactam substrate nitrocefin (NCF) for ADC-7 were determined from initial steady-state velocities using this colorimetric indicator (NCF, $\Delta\varepsilon_{482}$ = 17400 M^{-1} cm^{-1}). The kinetic parameters for ADC-7 were obtained using iterative nonlinear least-squares fit of the data to the Henri-Michaelis equation using GraphPad Prism 6.0 according to eq 1:

$$v = V_{max}[S]/(K_m + [S]) \quad (1)$$

Presently, the experimental evidence suggests that the inactivation of β-lactamases by BATSIs proceeds along the following mechanism,[38] where E is the enzyme, I is the BATSI, E:I represents an equilibrium binding complex, and E-I* represents a covalent, reversible complex that mimics either the acylation or deacylation transition state observed in the hydrolysis of a typical β-lactam substrate:[39−41]

$$E + I \rightleftharpoons E{:}\ I \rightleftharpoons E\text{-}I^*$$

The K_i for the BATSI inhibitors was determined by measuring initial steady-state velocities in the presence of a constant concentration of enzyme (2 nM) with increasing concentrations of inhibitor against the indicator substrate NCF (60 μM). In all assays, the measurements of initial velocities were performed with the addition of NCF after a 5 min preincubation of enzyme with inhibitor, as described in previous studies.[15,40,42−44] The average velocities (v_0) were then fitted to eq 2, where v_u represents the reporter's (NCF) uninhibited velocity and K_i(observed) represents the inhibitor concentration that results in a 50% reduction of v_u.

$$v_0 = v_u - ((v_u[I])/(K_i(\text{observed}) + [I])) \quad (2)$$

K_i values were corrected for nitrocefin affinity (K_m = 21.2 μM) according to eq 3:

$$K_i(\text{corrected}) = K_i(\text{observed})/(1 + [NCF]/K_{mNCF}) \quad (3)$$

Circular Dichroism (CD). Thermal denaturation and stability CD experiments were performed in a Jasco J-815 spectrometer (Easton, MD) with a Peltier effect temperature controller (GE Healthcare, Piscataway, NJ). Quartz cells with a 0.1 cm path length (Hellma, New York) were used for all experiments. Spectra were obtained with an ADC-7 concentration of 10 μM. Compounds were tested at a concentration of 200 μM to ensure that they did not interfere with the refraction of the light by the protein in the far UV spectrum.

Thermal melting was performed between 22 and 75 °C with a heating rate of 2 °C/min. Raw equilibrium denaturation data, monitored by far-UV CD at 221 nm, were normalized to the fraction of denatured protein (f_u), and the data were used for calculations of melting temperature T_m (see Supplementary Figure 2, Supporting Information). To determine if the thermal denaturation of ADC-7 follows a two-state process, the sample was monitored for changes in tertiary structure in the near-UV region, at 270 nm (data not shown), as previously described by Beadle et. al.[45] The melting for near-UV CD was performed using 30 μg/mL ADC-7 and a heating rate of 2 °C/min.

Thermodynamic Parameters Determination by Isothermal Titration Calorimetry (ITC). ITC experiments for investigation of the binding affinity of ADC-7 for BATSIs were performed using a MicroCal (GE Healthcare) VP-ITC microcalorimeter. All measurements were taken at 25 °C in 10 mM phosphate buffer (pH 7.4). ADC-7 β-lactamase and all ligand solutions were prepared in the same phosphate buffer (see Supplementary Figure 3 for a representative binding reaction of ADC-7 with SM23).

The protein concentration was determined using ε_{280} of 46 300 M^{-1} cm^{-1}, and the concentration of the BATSI was determined by weight. The 1.47 mL sample cell was filled with a 9−12 μM protein solution and the 300 μL injection syringe with a 0.25−0.5 mM BATSI solution that was injected at a rate of 5 μL every 210 s into the sample cell. All titrations were performed with a stirring speed of 307 rpm. The initial injection was not used for data fitting. Titrations were run past the point of enzyme saturation to determine and correct for heat of dilution. The data were fit using the One Set of Sites model provided with Origin 7.0 to determine K_a ($1/K_D$),ΔH, ΔS, and n (number of sites). The raw ITC data represent the heat generated by the enzyme upon converting n moles of substrate to product and is dependent on the M_t (free concentration of the enzyme), X_t (free concentration of the ligand), θ (fraction of sites occupied by ligand), and the V_0 (sample cell volume).[46−49] The Gibbs free energy ΔG was calculated with eq 4.

$$\Delta G = \Delta H - T\Delta S \quad (4)$$

RESULTS

Kinetics, Biophysical Characterization, and Microbiology. In order to assess the binding affinity of ADC-7 with the two boronic acid transition state inhibitors, S02030 and SM23, kinetic analyses were performed using nitrocefin as an indicator substrate. As shown in Table 1, both compounds were potent inhibitors of ADC-7 and demonstrated relatively high binding affinity to the enzyme (SM23: K_i = 21.1 ± 1.9 nM; S02030: K_i = 44.5 ± 2.2 nM).

dx.doi.org/10.1021/bi500887n | *Biochemistry* 2014, 53, 7670−7679

Along with the kinetic analyses that demonstrated that SM23 and S02030 can inhibit the ability of ADC-7 to hydrolyze nitrocefin, thermal stability and thermodynamic analysis were applied to further understand the contributions of the R1 and R2 side chains to binding. Investigating the changes in enthalpy (ΔH) and entropy (ΔS) of binding energy can provide insights into the optimization of side chain interactions to increase the affinity (K_D) between an enzyme and new ligands. In the case of SM23 and S02030 (Table 1), both compounds have favorable enthalpies (ΔH_{SM23} = −5.4 ± 0.3 kcal/mol and ΔH_{S02030} = −9.3 ± 0.5 kcal/mol) and relative similar binding energies (ΔG_{SM23} = −9.61 ± 0.5 kcal/mol and ΔG_{S02030} = −8.51 ± 0.3 kcal/mol). For S02030, which has a slightly less favorable binding energy than SM23 (~0.7 kcal/mol), the higher enthalpy compensates for the loss in entropy (ΔS_{SM23} = 14.1 ± 0.5 cal/mol·K, vs ΔS_{S02030} = −2.76 ± 0.1 cal/mol·K). This examination suggests that enthalpically driven compounds may be optimized by introducing additional conformational constraints and/or hydrophobic groups.

Representative two-state thermal denaturation of ADC-7 with and without the inhibitors was monitored by far-UV CD at 221 nm (Figure S2A). The melting temperature (T_m) for ADC-7 was ~61 ± 1 °C at 221 nm (60 ± 1 °C at 270 nm), and for the complexes, the T_m was ~64 ± 1 °C and ~65 ± 1 °C for SM23 and S02030, respectively. These melting temperatures were similar for far-UV and near-UV spectrum, suggesting two-state thermal denaturation. Comparison of the CD spectrum of ADC-7 with that of ADC-7/SM23 showed differences in signal ellipticity that suggests subtle conformational changes induced by the inhibitor upon binding (Figure S2B).

To test if the inhibitors were active against bacteria expressing ADC-7, disc susceptibility assays (DSAs) were performed and MIC values were determined. In a uniform *E. coli* DH10B genetic background, excellent inhibition of ADC-7 β-lactamase by the BATSIs is observed at a concentration of 10 μg/mL when coupled with the β-lactam ceftazidime (CAZ; Table 2). The DSA zone sizes increased from 12 mm for CAZ alone to 25 and 26 mm for SM23 and S02030, respectively. An achiral BATSI that contains the R1 side chain found in SM23 and S02030 but lacks an R2 side chain was also tested to explore the importance of the R2 side chain (Figure 1C). For the achiral BATSI, the zone size was also increased, but not as substantially as with the chiral BATSIs (17 mm vs 25 and 26 mm). Using a fixed concentration of the BATSIs (4 μg/mL), the MIC values were shown to decrease from 64 μg/mL to 8 μg/mL (for SM23 and S02030) and 32 μg/mL (for the achiral BATSI) (Table 3). In an *A. baumannii* background (strain M9 from which bla_{ADC} was initially cloned), we also see a reduction of MIC values from >64 to 16 μg/mL for S02030. The latter result is most encouraging as the lack of permeability across the outer membrane of *A. baumannii* is a significant challenge in medicinal chemistry.

Table 2. Disc Susceptibility Assays (DSAs), in mm

	E. coli DH10B bla_{ADC-7} (mm)
no antibiotic	6
CAZ − 10 μg	12
CAZ + 10 μg achiral cephalothin	17
CAZ + 10 μg SM23	25
CAZ + 10 μg S02030	26

Table 3. MIC Values (μg/mL) in Combination with 4 μg/mL BATSI Compound

strain	CAZ	CAZ S02030	CAZ SM23	CAZ achiral cephalothin
E. coli DH10B	1	0.25	0.5	0.5
E. coli DH10B pBCSK, bla_{ADC-7}	64	8	8	32
A. baumannii M9	>64	16	32	32

X-ray Crystal Structures of apo ADC-7 and in Complex with Boronic Acid Inhibitor S02030. The structure of apo ADC-7 was determined to 1.73 Å resolution (Figure 2; Table 4). ADC-7 crystallized in the *P*1 space group with eight molecules in the asymmetric unit. A phosphate ion was observed in the active sites of each of the eight monomers of the asymmetric unit (Figure 2). The quality of the final model was evaluated with MolProbity.[50] In this model, 97.1% of all residues were in the favored region of the Ramachandran plot, and 99.9% were in the allowed region. The final *R* and R_{free} were 19.6% and 24.0%, respectively, and the coordinates and structure factors have been deposited in the Protein Data Bank as 4U0T. The overall fold of ADC-7 is a mixed α/β structure and resembles that observed in other class C β-lactamases, including the recently determined structure of ADC-1.[51]

To better understand the structural basis for inhibition of ADC-7 by BATSIs, the X-ray crystal structure of the ADC-7/S02030 complex was determined to 2.03 Å resolution (Figure 3; Table 4). The complex was obtained by soaking the inhibitor into preformed ADC-7 crystals. The space group was $P2_1$, with four molecules in the asymmetric unit. Inspection of the initial $F_o - F_c$ maps contoured at 3σ showed unambiguous electron density for the inhibitor bound in the active site of all four molecules. The density was contiguous with the Oγ atom of Ser64, suggesting that the inhibitor was covalently attached to the catalytic serine residue. The inhibitor molecule was built into the density in all active sites and further refined with Refmac5. $2F_o - F_c$ maps calculated from the refined model confirmed the covalent attachment to Ser64. A tetrahedral geometry was observed around the boron atom of the inhibitor. In addition to the four inhibitors, the final model of the complex contained 1,421 protein residues and 668 water molecules. The final *R* and R_{free} were 19.6% and 24.0%, respectively, and the coordinates and structure factors have been deposited in the Protein Data Bank as 4U0X.

The quality of the model was analyzed with MolProbity, with 96.2% of all of the residues found in the favored region of the Ramachandran plot and 99.7% in the allowed region. B factors for each of the monomers were calculated with Moleman2,[52] and these values ranged from 23.5 Å^2 (B monomer) to 41.4 Å^2 (D monomer).

Superposition of each of the monomers reveals that S02030 binds in similar, but not identical, orientations in each of the sites (Figure 4). The overall conformation of the inhibitors is the same with the R1 and R2 groups forming favorable intramolecular van der Waals interactions. Other similarities include the tetrahedral geometry around the boron atom and the position of the R1 group in the active site that is analogous to where the R1 side chains of β-lactam substrates bind in other class C β-lactamases. The O1 hydroxyl group is positioned in the oxyanion hole and makes a favorable hydrogen bond with the main chain nitrogen of Ser315 (2.8 Å) and long hydrogen bonds to the main chain nitrogen of Ser64 and main chain oxygen of Ser315 (3.2−3.4 Å). The R1 amide group interacts with the side chain nitrogens of Gln120 and Asn152 and the main chain oxygen of Ser315. The thiophene ring in the R1

dx.doi.org/10.1021/bi500887n | *Biochemistry* 2014, 53, 7670−7679

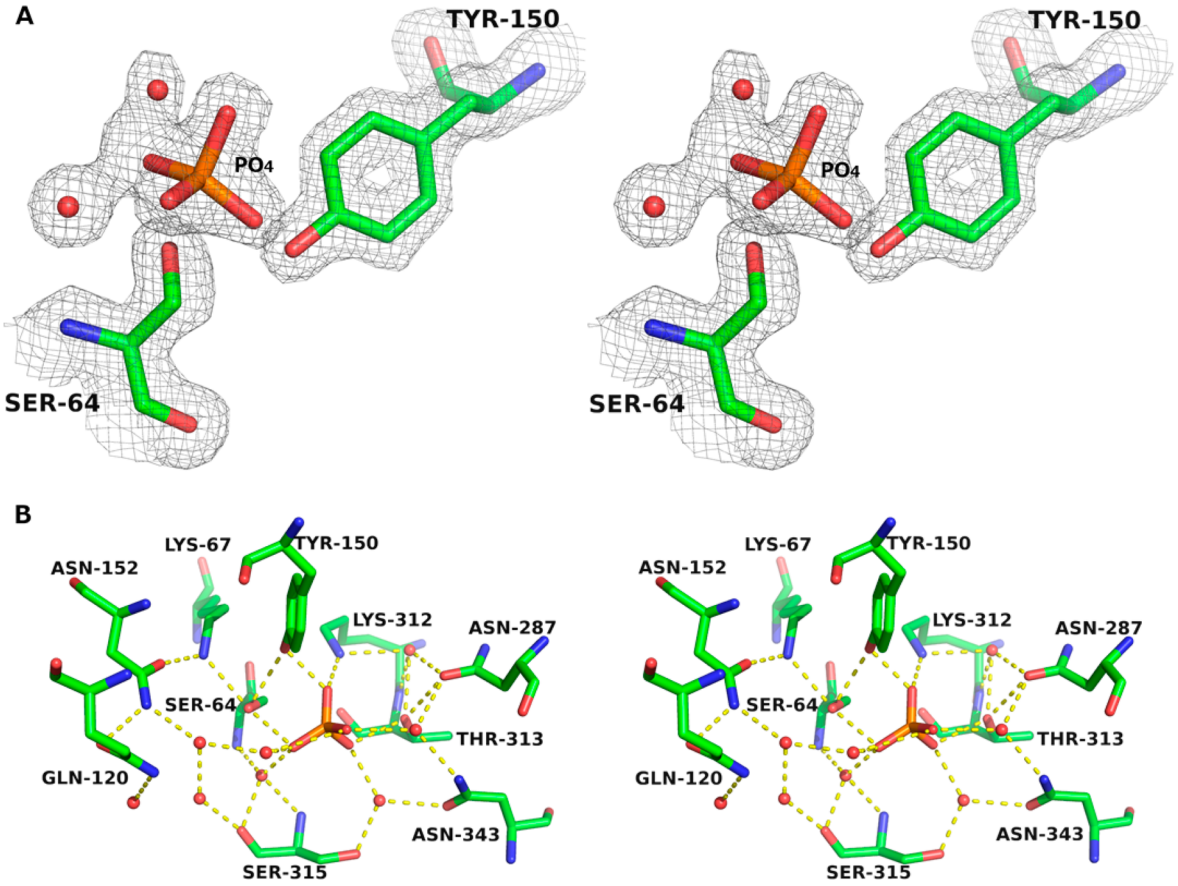

Figure 2. Stereoview of the ADC-7 active site. (A) The $2F_o - F_c$ electron density map is contoured at 1.0 σ and colored gray. (B) Hydrogen bonding interactions observed between active site residues, water molecules, and phosphate ion. Hydrogen bonds are shown as yellow dashed lines and represent distances between 2.4−3.2 Å. Water molecules are indicated with red spheres. Carbon atoms of the active site residues are colored green, oxygens red, and nitrogens blue. The phosphorus of the phosphate is colored orange. This and all subsequent figures were made with PyMOL.[59]

side chain is in an identical conformation in the B and D monomers. In the C monomer the ring is rotated approximately 180° around the C12−C13 bond from the orientation observed in A and D monomers. Electron density supports the existence of two alternate conformations for the ring in the A monomer. One is the same as the conformation in monomers A and D, and the other differs by an approximate 120° rotation around C12−C13. Regardless, the thiophene ring is not involved in any significant interactions with the enzyme.

Where larger differences are observed is in the position of the inhibitor R2 group. In two of the monomers (A and C), the R2 carboxytriazole groups are in similar positions, interacting favorably with Arg340 (~2.6−3.3 Å). The inhibitor in the D monomer is rotated approximately 150° around C7−C8, placing its carboxylate group in a different region of the active site; the carboxylate carbon atom (C21) has moved ~4.5 Å from its position in the A and C monomers. Yet the R2 group still maintains interactions with Arg340 in one of two observed alternate conformations for this residue. In the A monomer, the R2 group has rotated to an intermediate position between the B/C and D locations, with the C21 atom displaced 3.6 Å from its position in B/C and 2.1 Å from its D position.

DISCUSSION

ADC-7 is a class C β-lactamase target in the clinically relevant *Acinetobacter* spp. Here we show that BATSIs SM23 and S02030 bind to ADC-7 with high affinity and have the ability to act synergistically with β-lactams to overcome resistance in bacteria that express ADC-7. This is extremely encouraging as the penetration of both antibiotics and inhibitors into the cell represents a significant challenge in medicinal chemistry.

Boronic acids present a starting point for the development of this class of molecules as novel inhibitors in the particularly troublesome species. In this context, we could exploit the potential of click chemistry as a powerful tool in drug discovery. The term "click" is reserved to the "near-perfect" reaction, and CuCAAC is the click reaction *par excellence*. The high degree of dependability and flexibility of this method allows for the rapid synthesis of compound libraries for SAR profiling, accelerating both lead identification and optimization.[53−55] From a synthetic point of view, the application of CuCAAC was a key step in obtaining the compound S02030 and offers potentially easy access to a wide range of substituted triazoles, useful not only for further exploration of structure−activity relationship, but also for enhanced cell penetration. In our case, from the key 2-azido-1-acylamino-ethaneboronate intermediate **5**, we have the opportunity to generate a library of new BATSIs exploring different substituents on the triazole ring, with terminal acetylene accessibility the only potential limitation.

Importantly, BATSIs do not resemble β-lactams, and yet SM23 and S02030 bind with high affinity to ADC-7 (K_i values of 21.1 and 44.5 nM, respectively). The original intent for determining the ADC-7/S02030 complex was to understand the interactions responsible for this affinity. AmpC has been

dx.doi.org/10.1021/bi500887n | *Biochemistry* 2014, 53, 7670−7679

Table 4. Crystallographic Summary for the apo Structure of ADC-7 and Its Complex with S02030

	ADC-7 apo	ADC-7/S02030
cell constants (Å; °)	a = 81.00, b = 88.57, c = 105.88	a = 89.27, b = 81.20, c = 106.33
	α = 67.29, β = 89.84, γ = 89.40	$\alpha = \gamma$ = 90, β = 113.08
space group	$P1$	$P2_1$
resolution (Å)	1.73 (1.81−1.73)[a]	2.02 (2.03−2.02)
unique reflections	273490	91079
total observations	784216	691655
R_{merge} (%)	6.5 (40.0)	8.7 (64.9)
completeness (%)[b]	97.3 (95.9)	100 (99.9)
$<I/\sigma_I>$	8.45 (3.07)	17.6 (3.3)
resolution range for refinement (Å)	40−1.73	50−2.03
number of protein residues	2,820	1,421
number of water molecules	1,580	668
number of phosphates	8	1
RMSD bond lengths (Å)	0.019	0.016
RMSD bond angles (deg)	1.999	1.840
R-factor (%)	19.6	18.5
R_{free} (%)[c]	24.0	24.8
average B-factor, protein atoms (Å^2)	17.8	34.0
average B-factor, drug atoms (Å^2)	n/a	45.2
average B-factor, water molecules (Å^2)	28.2	35.6
average B-factor, phosphates (Å^2)	22.2	67.5

[a]Values in parentheses are for the highest resolution shell. [b]Fraction of theoretically possible reflections observed. [c]R_{free} was calculated with 5% of reflections set aside randomly.

extensively characterized with respect to inhibition by boronic acids.[56] Many of these interactions identified in AmpC/BATSI

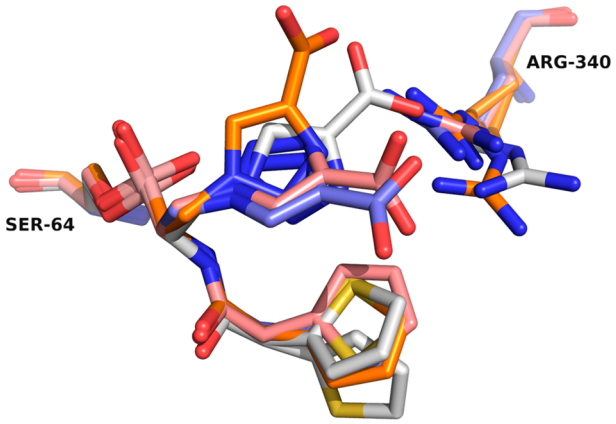

Figure 4. Overlay of the S02030 inhibitor conformations in all four ADC-7 active sites. The R1 side chain binds similarly in all four conformations. Differences arise in the placement of the inhibitor R2 group (carboxytriazole) and its interaction with Arg340. In monomers B (purple) and C (salmon), the R2 group adopts similar conformations and interacts with Arg340, which is observed in a single conformation. In monomers A (white) and D (orange), the conformations of the inhibitor are somewhat different, and alternate and/or multiple conformations of Arg340 are also observed.

complexes are conserved in the ADC-7 complex with S02030, for example the oxyanion/hydroxyl hole and the R1 amide recognition site. These features are likely to be generally applicable to boronic acid inhibition of ADC enzymes.

The next step is to improve the properties of S02030 so that the high affinity also translates into increased activity against resistant bacteria. Unlike the achiral cephalothin BATSI from which they are derived, SM23 and S02030 contain both an R1 and an R2 group (Figure 1C). These two regions are important for exploring different areas of the active site, as well as for identifying important inhibitor recognition sites to aid in future

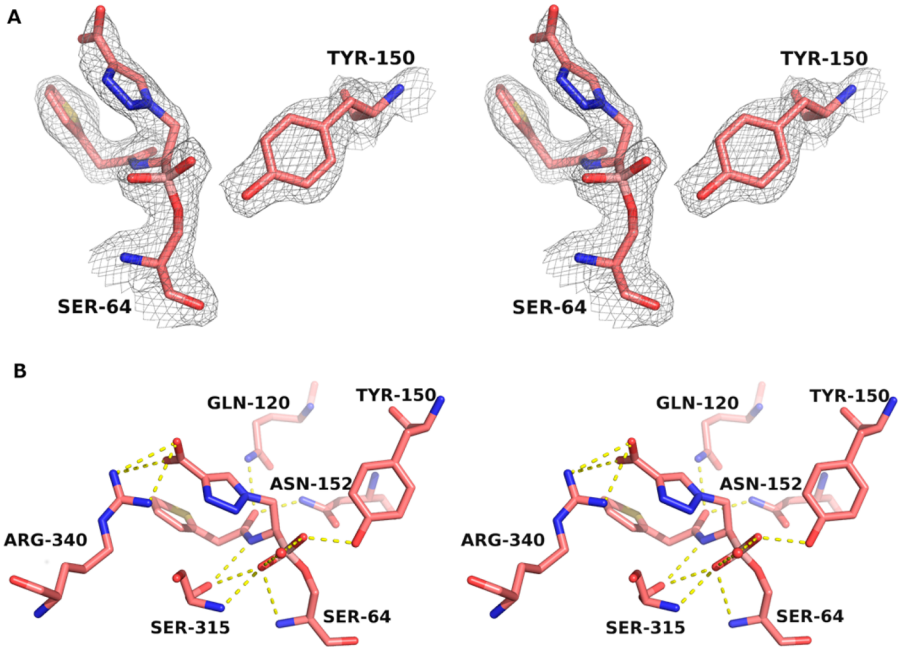

Figure 3. Stereoview of the ADC-7/S02030 complex. (A) The $2F_o - F_c$ electron density map is contoured at 1.0 σ and colored gray. (B) Hydrogen bonding interactions observed between ADC-7 and the boronic acid inhibitor S02030. The active site shown is the C monomer (the inhibitor in the B monomer binds similarly). Hydrogen bonds and ionic interactions are shown as yellow dashed lines and represent distances between 2.6−3.3 Å. Water molecules are indicated with red spheres. Carbon atoms of the active site residues are colored salmon, oxygens red, nitrogens blue, sulfurs yellow, and boron is light pink.

dx.doi.org/10.1021/bi500887n | *Biochemistry* 2014, 53, 7670−7679

optimization efforts. Focusing first on the R2 group, the ADC-7/S02030 complex showed differences in S02030 binding, coupled with multiple Arg340 conformations (Figure 4) in each of the four monomers of ADC-7. This lack of a single consensus binding mode for the inhibitor suggests that the R2 carboxylate group of S02030 may be too close to Arg340, resulting in a steric clash between this residue and the carboxylate group of the inhibitor. From the AmpC/SM23 (PDB 1MXO) comparison, removal of the carbon linker may place the carboxylate in an ideal position for a favorable interaction with Arg340 (Figure 5). The shorter R2 group of SM23 may allow for a favorable and stabilizing interaction with Arg340 and may explain why SM23 has a higher affinity for ADC-7.

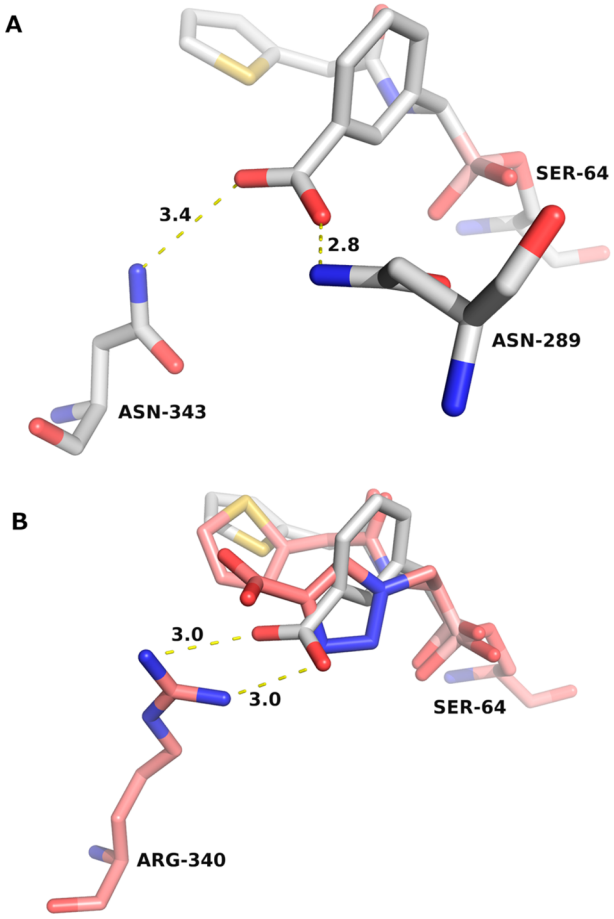

Figure 5. Superposition of ADC-7/S02030 (salmon) complex with AmpC/SM23 (white). Boronic acid inhibitor (SM23) is bound to the AmpC active site and highlights the position of the inhibitor's carboxylate group that is meant to mimic the corresponding group common to β-lactams.

Given the notable absence of favorable interactions with the R1 group of S02030, an obvious next step to potentially optimize S02030 is to introduce favorable interactions in this region. Several residues in this region offer the possibility of making more productive interactions with an inhibitor. For example, Gln120 and Ser317 are both located near the thiophene ring of S02030. Addition of a carboxylate group or a tetrazole ring in this region might allow for interactions with one or both of these residues. Both of these additions have been shown to improve the affinity of related BATSIs.[57,58] Additionally, replacing the thiophene ring with a phenyl ring might introduce favorable quadrupole−quadrupole interactions with Tyr222, another feature important for recognition of arylboronic acids by other class C enzymes.[56]

In closing, there is a pressing need for the development of novel inhibitors for the class C enzymes in *Acinetobacter* spp. to overcome β-lactam mediated resistance. These initial BATSIs provide an excellent starting point with high binding affinities for ADC-7 and antimicrobial activity against resistant bacteria expressing ADC-7. Analysis of the first structure of an ADC enzyme in complex with a BATSI suggests areas that could be exploited in these optimization efforts. Interestingly, the applications of thermodynamic parameters in the analysis of these reversible inhibitors represent another approach to improve inhibitor design. Here, we see early indications that enthalpies can be a driving force in enzyme−inhibitor interactions. The data derived from ITC and CD provide a thermodynamic basis for the SAR of the newly described inhibitors and nicely complement the data derived from the X-ray crystal structures. This more complete understanding of the SAR will guide future strategies for novel BATSI analogue design.

■ ASSOCIATED CONTENT

Supporting Information

Supporting Information (NMR spectra) is available for intermediates **4**, **5**, **6**, and the final product S02030 (Figure S1). In addition, representative CD and ITC experiments are shown in Figures S2 and S3. This material is available free of charge via the Internet at http://pubs.acs.org.

■ AUTHOR INFORMATION

Corresponding Authors

*(B.W.) E-mail: wallarb@gvsu.edu. Phone: 616-331-3807

*(R.A.B.) E-mail: robert.bonomo@va.gov. Phone: 216-791-3800 ext 4645.

Funding

This work was supported in part by funds and/or facilities provided by the Cleveland Department of Veterans Affairs, the Department of Veterans Affairs Merit Review Program 1I01BX001974, the Veterans Integrated Service Network 10 Geriatric Research, Education, and Clinical Center (VISN 10 GRECC), and the National Institute of Allergy and Infectious Diseases of the National Institutes of Health under Award Numbers R01 AI100560 and R01 AI063517. Use of the Advanced Photon Source, an Office of Science User Facility operated for the U.S. Department of Energy (DOE) Office of Science by Argonne National Laboratory was supported by the U.S. DOE under Contract No. DE-AC02-06CH11357. Use of the LS-CAT Sector 21 was supported by the Michigan Economic Development Corporation and the Michigan Technology Tri-Corridor (Grant 085P1000817).

Notes

The authors declare no competing financial interest.

■ ACKNOWLEDGMENTS

As a Student Summer Scholar in the Office of Undergraduate Research at Grand Valley State University, H.C.S. was supported by the MaryBeth Koeze Endowed Fellowship in memory of Dr. Thomas Henry Koeze. We thank Zachary Garlets for assistance with the first crystallization trials of ADC-7 and the Centro Interdipartimentale Grandi Strumenti of Modena for NMR and MS spectra.

■ ABBREVIATIONS

ADC, *Acinetobacter*-derived cephalosporinase; BLI, β-lactamase inhibitors; PBP, penicillin binding protein; DBO, diazabicyclo-[3.2.1]octanone; BATSI, boronic acid transition state inhibitor; CuCAAC, copper catalyzed azide alkyne cycloaddition; DSA, disc susceptibility assay; MIC, minimum inhibitory concentrations; LS-CAT, life sciences collaborative access team; NCF, nitrocefin; ITC, isothermal calorimetry; CD, circular dichroism; SSM, secondary structure matching; RMSD, root-mean-square deviation; CAZ, ceftazidime; MDR, multidrug resistant

■ REFERENCES

(1) Bonomo, R. A., and Szabo, D. (2006) Mechanisms of multidrug resistance in *Acinetobacter* species and *Pseudomonas aeruginosa*. *Clin. Infect. Dis. 43* (Suppl 2), S49−56.

(2) Perez, F., Endimiani, A., and Bonomo, R. A. (2008) Why are we afraid of *Acinetobacter baumannii*? *Expert Rev. Anti-Infect. Ther. 6*, 269−271.

(3) Perez, F., Endimiani, A., Ray, A. J., Decker, B. K., Wallace, C. J., Hujer, K. M., Ecker, D. J., Adams, M. D., Toltzis, P., Dul, M. J., Windau, A., Bajaksouzian, S., Jacobs, M. R., Salata, R. A., and Bonomo, R. A. (2010) Carbapenem-resistant *Acinetobacter baumannii* and *Klebsiella pneumoniae* across a hospital system: impact of post-acute care facilities on dissemination. *J. Antimicrob. Chemother. 65*, 1807−1818.

(4) Perez, F., Hujer, A. M., Hujer, K. M., Decker, B. K., Rather, P. N., and Bonomo, R. A. (2007) Global challenge of multidrug-resistant Acinetobacter baumannii. *Antimicrob. Agents Chemother. 51*, 3471−3484.

(5) Wright, M. S., Haft, D. H., Harkins, D. M., Perez, F., Hujer, K. M., Bajaksouzian, S., Benard, M. F., Jacobs, M. R., Bonomo, R. A., and Adams, M. D. (2014) New insights into dissemination and variation of the health care-associated pathogen Acinetobacter baumannii from genomic analysis. *mBio 5*, e00963−00913.

(6) Perez, F., Endimiani, A., Hujer, K. M., and Bonomo, R. A. (2007) The continuing challenge of ESBLs. *Curr. Opin. Pharmacol. 7*, 459−469.

(7) Drawz, S. M., and Bonomo, R. A. (2010) Three decades of beta-lactamase inhibitors. *Clin. Microbiol. Rev. 23*, 160−201.

(8) Drawz, S. M., Papp-Wallace, K. M., and Bonomo, R. A. (2014) New beta-lactamase inhibitors: a therapeutic renaissance in an MDR world. *Antimicrob. Agents Chemother. 58*, 1835−1846.

(9) Bou, G., Santillana, E., Sheri, A., Beceiro, A., Sampson, J. M., Kalp, M., Bethel, C. R., Distler, A. M., Drawz, S. M., Pagadala, S. R., van den Akker, F., Bonomo, R. A., Romero, A., and Buynak, J. D. (2010) Design, synthesis, and crystal structures of 6-alkylidene-2′-substituted penicillanic acid sulfones as potent inhibitors of Acinetobacter baumannii OXA-24 carbapenemase. *J. Am. Chem. Soc. 132*, 13320−13331.

(10) Hujer, K. M., Hamza, N. S., Hujer, A. M., Perez, F., Helfand, M. S., Bethel, C. R., Thomson, J. M., Anderson, V. E., Barlow, M., Rice, L. B., Tenover, F. C., and Bonomo, R. A. (2005) Identification of a new allelic variant of the Acinetobacter baumannii cephalosporinase, ADC-7 beta-lactamase: defining a unique family of class C enzymes. *Antimicrob. Agents Chemother. 49*, 2941−2948.

(11) Perichon, B., Goussard, S., Walewski, V., Krizova, L., Cerqueira, G., Murphy, C., Feldgarden, M., Wortman, J., Clermont, D., Nemec, A., and Courvalin, P. (2014) Identification of 50 class D beta-lactamases and 65 Acinetobacter-derived cephalosporinases in Acinetobacter spp. *Antimicrob. Agents Chemother. 58*, 936−949.

(12) Snitkin, E. S., Zelazny, A. M., Montero, C. I., Stock, F., Mijares, L., Program, N. C. S., Murray, P. R., and Segre, J. A. (2011) Genome-wide recombination drives diversification of epidemic strains of *Acinetobacter baumannii*. *Proc. Natl. Acad. Sci. U. S. A. 108*, 13758−13763.

(13) Drawz, S. M., Babic, M., Bethel, C. R., Taracila, M., Distler, A. M., Ori, C., Caselli, E., Prati, F., and Bonomo, R. A. (2010) Inhibition of the class C beta-lactamase from Acinetobacter spp.: insights into effective inhibitor design. *Biochemistry 49*, 329−340.

(14) Tian, G. B., Adams-Haduch, J. M., Taracila, M., Bonomo, R. A., Wang, H. N., and Doi, Y. (2011) Extended-spectrum AmpC cephalosporinase in Acinetobacter baumannii: ADC-56 confers resistance to cefepime. *Antimicrob. Agents Chemother. 55*, 4922−4925.

(15) Morandi, F., Caselli, E., Morandi, S., Focia, P. J., Blazquez, J., Shoichet, B. K., and Prati, F. (2003) Nanomolar inhibitors of AmpC beta-lactamase. *J. Am. Chem. Soc. 125*, 685−695.

(16) Davoli, P., Fava, R., Morandi, S., Spaggiari, A., and Prati, F. (2005) Enantioselective total synthesis of (−)-microcarpalide. *Tetrahedron 61*, 4427−4436.

(17) Matteson, D. S., Maliakal, D., and Fabry-Asztalos, L. (2008) Synthesis of a (β-acetamido-α-acetoxyethyl)boronic ester via azido boronic esters. *J. Organomet. Chem. 693*, 2258−2262.

(18) Lipshutz, B. H., and T, B. R. (2006) Heterogeneous copper-in-charcoal-catalyzed click chemistry. *Angew. Chem. 118*, 8415−8418.

(19) Matteson, D. S. (1988) Asymmetric synthesis with boronic esters. *Acc. Chem. Res. 21*, 294−300.

(20) Matteson, D. S. (1989) Alpha-haloboronic esters: intermediates for stereodirected synthesis. *Chem. Rev. 89*, 1535−1551.

(21) Matteson, D. S. (1999) Functional group compatibilities in boronic ester chemistry. *Organometallic Chem. 581*, 51−65.

(22) Matteson, D. S., Ray, R., Rocks, R. R., and Tsai, D. J. S. (1983) Directed chiral synthesis by way of α-chloro boronic esters. *Organometallics 2*, 1536−1543.

(23) Kappe, C. O., and Van der Eycken, E. (2010) Click chemistry under non-classical reaction conditions. *Chem. Soc. Rev. 39*, 1280−1290.

(24) Meldal, M., and Tornøe, C. W. (2008) Cu-catalyzed azide-alkyne cycloaddition. *Chem. Rev. 108*, 2952−3015.

(25) Rostovtsev, V. V., Green, L. G., Fokin, V. V., and Sharpless, K. B. (2002) A stepwise Huisgen cycloaddition process: copper(I)-catalyzed regioselective ligation of azides and terminal alkynes. *Angew. Chem. Int. Ed 41*, 2596−2599.

(26) Wityak, J., Earl, R. A., Abelman, M. M., Bethel, Y. B., Fisher, B. N., Kauffman, G. S., Kettner, C. A., Ma, P., McMillan, J. L., Mersinger, L. J., Pesti, J., Pierce, M. E., Rankin, W. F., Chorvat, R. J., and Confalone, P. N. (1995) Synthesis of thrombin inhibitor DuP 714. *J. Org. Chem. 60*, 3717−3722.

(27) Prati, F., and Caselli, E. (2013) Boronic acid inhibitors of beta-lactamases as therapeutic agents in treatment of antibiotic-resistant infection diseases. *PCT Int. Appl.* (2013), WO 2013053372 A1 20130418.

(28) Clinical and Laboratory Standards Institute. (2007) *Performance Standards for Antimicrobial Susceptibility Testing*; Seventeenth Informational Supplement, Vol. 27.

(29) Gasteiger, E. H. C., Gattiker, A., Duvaud, S., Wilkins, M. R., Appel, R. D., Bairoch, A. (2005) Protein Identification and Analysis Tools on the ExPASy Server, In *The Proteomics Protocols Handbook* (Walker, J. M., Ed.) pp 571−607, Humana Press, New York.

(30) Otwinowski, Z., and Minor, W. (1997) Processing of X-ray diffraction data collected in oscillation mode. *Methods Enzymol. 276*, 307−326.

(31) Kabsch, W. (2010) *Acta Crystallogr. D Biol. Crystallogr. 66*, 125−132.

(32) McCoy, A. J., Grosse-Kunstleve, R. W., Adams, P. D., Winn, M. D., Storoni, L. C., and Read, R. J. (2007) Phaser crystallographic software. *J. Appl. Crystallogr. 40*, 658−674.

(33) Kelley, L. A., and Sternberg, M. J. (2009) Protein structure prediction on the Web: a case study using the Phyre server. *Nat. Protoc. 4*, 363−371.

(34) Michaux, C., Massant, J., Kerff, F., Frere, J. M., Docquier, J. D., Vandenberghe, I., Samyn, B., Pierrard, A., Feller, G., Charlier, P., Van Beeumen, J., and Wouters, J. (2008) Crystal structure of a cold-adapted class C beta-lactamase. *FEBS J. 275*, 1687−1697.

(35) Murshudov, G. N., Vagin, A. A., and Dodson, E. J. (1997) Refinement of macromolecular structures by the maximum-likelihood method. *Acta Crystallogr. D Biol. Crystallogr. 53*, 240−255.

(36) CCP4 (Collaborative Computational Project Number 4) (1994) The CCP4 suite: programs for protein crystallography. *Acta Crystallogr., Sect. D 50*, 760−763.
(37) Emsley, P., and Cowtan, K. (2004) Coot: Model-building tools for molecular graphics. *Acta Crystallogr. D 60*, 2126−2132.
(38) Crompton, I. E., Cuthbert, B. K., Lowe, G., and Waley, S. G. (1988) Beta-lactamase inhibitors. The inhibition of serine beta-lactamases by specific boronic acids. *Biochem. J. 251*, 453−459.
(39) Bulychev, A., Massova, I., Miyashita, K., and Mobashery, S. (1997) Nuances of mechanisms and their implications for evolution of the versatile beta-lactamase activity: From biosynthetic enzymes to drug resistance factors. *J. Am. Chem. Soc. 119*, 7619−7625.
(40) Chen, Y., Shoichet, B., and Bonnet, R. (2005) Structure, function, and inhibition along the reaction coordinate of CTX-M beta-lactamases. *J. Am. Chem. Soc. 127*, 5423−5434.
(41) Powers, R. A., Blazquez, J., Weston, G. S., Morosini, M. I., Baquero, F., and Shoichet, B. K. (1999) The complexed structure and antimicrobial activity of a non-beta-lactam inhibitor of AmpC beta-lactamase. *Protein Sci. 8*, 2330−2337.
(42) Morandi, S., Morandi, F., Caselli, E., Shoichet, B. K., and Prati, F. (2008) Structure-based optimization of cephalothin-analogue boronic acids as beta-lactamase inhibitors. *Bioorg. Med. Chem. 16*, 1195−1205.
(43) Thomson, J. M., Distler, A. M., Prati, F., and Bonomo, R. A. (2006) Probing active site chemistry in SHV beta-lactamase variants at Ambler position 244. Understanding unique properties of inhibitor resistance. *J. Biol. Chem. 281*, 26734−26744.
(44) Wang, X., Minasov, G., Blazquez, J., Caselli, E., Prati, F., and Shoichet, B. K. (2003) Recognition and resistance in TEM beta-lactamase. *Biochemistry 42*, 8434−8444.
(45) Beadle, B. M., McGovern, S. L., Patera, A., and Shoichet, B. K. (1999) Functional analyses of AmpC beta-lactamase through differential stability. *Protein Sci. 8*, 1816−1824.
(46) Ladbury, J. E. (2010) Calorimetry as a tool for understanding biomolecular interactions and an aid to drug design. *Biochem. Soc. Trans. 38*, 888−893.
(47) Perozzo, R., Folkers, G., and Scapozza, L. (2004) Thermodynamics of protein-ligand interactions: history, presence, and future aspects. *J. Recept. Signal Transduction 24*, 1−52.
(48) Velazquez-Campoy, A., and Freire, E. (2006) Isothermal titration calorimetry to determine association constants for high-affinity ligands. *Nat. Protoc. 1*, 186−191.
(49) Velazquez-Campoy, A., Ohtaka, H., Nezami, A., Muzammil, S., and Freire, E. (2004) Isothermal titration calorimetry, in *Current Protocols in Cell Biology* (Bonifacino J. S. et al., Eds.) Chapter 17, Unit 17−18.
(50) Chen, V. B., Arendall, W. B., 3rd, Headd, J. J., Keedy, D. A., Immormino, R. M., Kapral, G. J., Murray, L. W., Richardson, J. S., and Richardson, D. C. (2010) MolProbity: all-atom structure validation for macromolecular crystallography. *Acta Crystallogr. D Biol. Crystallogr. 66*, 12−21.
(51) Bhattacharya, M., Toth, M., Antunes, N. T., Smith, C. A., and Vakulenko, S. B. (2014) Structure of the extended-spectrum class C beta-lactamase ADC-1 from Acinetobacter baumannii. *Acta Crystallogr. D Biol. Crystallogr. 70*, 760−771.
(52) Kleywegt, G. J. (1997) Validation of protein models from Calpha coordinates alone. *J. Mol. Biol. 273*, 371−376.
(53) Kolb, H. C., Finn, M. G., and Sharpless, K. B. (2001) Click Chemistry: Diverse Chemical Function from a Few Good Reactions. *Angew. Chem., Int. Ed. Engl. 40*, 2004−2021.
(54) Kolb, H. C., and Sharpless, K. B. (2003) The growing impact of click chemistry on drug discovery. *Drug Discovery Today 8*, 1128−1137.
(55) Moses, J. E., and Moorhouse, A. D. (2007) The growing applications of click chemistry. *Chem. Soc. Rev. 36*, 1249−1262.
(56) Powers, R. A., and Shoichet, B. K. (2002) Structure-based approach for binding site identification on AmpC beta-lactamase. *J. Med. Chem. 45*, 3222−3234.
(57) Eidam, O., Romagnoli, C., Dalmasso, G., Barelier, S., Caselli, E., Bonnet, R., Shoichet, B. K., and Prati, F. (2012) Fragment-guided design of subnanomolar beta-lactamase inhibitors active in vivo. *Proc. Natl. Acad. Sci. U. S. A. 109*, 17448−17453.
(58) Tondi, D., Morandi, F., Bonnet, R., Costi, M. P., and Shoichet, B. K. (2005) Structure-based optimization of a non-beta-lactam lead results in inhibitors that do not up-regulate beta-lactamase expression in cell culture. *J. Am. Chem. Soc. 127*, 4632−4639.
(59) *The PyMOL Molecular Graphics System*, Version 1.3, Schrödinger, LLC.